HHS Public Access

Author manuscript

*Neuron*. Author manuscript; available in PMC 2018 April 19.

Published in final edited form as:

*Neuron*. 2017 April 19; 94(2): 312–321.e3. doi:10.1016/j.neuron.2017.03.047.

# Assembly of excitatory synapses in the absence of glutamatergic neurotransmission

**Richard Sando**[1,2,3], **Eric Bushong**[4,5], **Yongchuan Zhu**[1,2,5], **Min Huang**[1,2,3,5], **Camille Considine**[1,2,5], **Sebastien Phan**[4], **Suyeon Ju**[4], **Marco Uytiepo**[1,2], **Mark Ellisman**[4,6], and **Anton Maximov**[1,2,6,7,*]

[1]Department of Neuroscience, The Scripps Research Institute, La Jolla, CA, USA

[2]The Dorris Neuroscience Center, The Scripps Research Institute, La Jolla, CA, USA

[3]The Kellogg School of Science and Technology, The Scripps Research Institute, La Jolla, CA, USA

[4]National Center for Microscopy and Imaging Research, University of California, San Diego, CA, USA

## SUMMARY

Synaptic excitation mediates a broad spectrum of structural changes in neural circuits across the brain. Here, we examine the morphologies, wiring, and architectures of single synapses of projection neurons in the murine hippocampus that developed in virtually complete absence of vesicular glutamate release. While these neurons had smaller dendritic trees and/or formed fewer contacts in specific hippocampal subfields, their stereotyped connectivity was largely preserved. Furthermore, loss of release did not disrupt the morphogenesis of presynaptic terminals and dendritic spines, suggesting that glutamatergic neurotransmission is unnecessary for synapse assembly and maintenance. These results underscore the instructive role of intrinsic mechanisms in synapse formation.

## INTRODUCTION

Wiring of the brain is strongly influenced by experience. Neurons in activated ensembles can dynamically change their morphologies, connectivity, and architectures of individual

*Correspondence to: amaximov@scripps.edu.
[5]These authors contributed equally
[6]Seniour author
[7]Lead contact

SUPPLEMENTAL INFORMATION

Supplemental information includes six figures, two tables, and two movies and can be found with this article online.

**AUTHOR CONTRIBUTIONS**

A.M. and R.S. conceived the study. R.S., Y.Z. and M.H. carried out electrophysiological, confocal imaging and biochemical experiments. C.C. traced single neurons and quantified synapse densities. M.Y. genotyped mice and assisted with histology. E.B., S. P. and S. J. prepared samples for EM and collected tomograms. M.E. supervised EM studies. A.M. wrote the manuscript.

synapses (Bourne and Harris, 2012; Espinosa and Stryker, 2012; Holtmaat and Svoboda, 2009; Sudhof and Malenka, 2008; Tonegawa et al., 2015). Nonetheless, animals and humans have innate behaviors (Kimchi et al., 2007; Papes et al., 2010), suggesting that many synaptic pathways are genetically predetermined. Such hardwiring has been documented in sensory systems (Pecho-Vrieseling et al., 2009), but the extent of intrinsic assembly of circuits essential for high order processing of sensory information, learning and memory storage remains poorly understood.

The importance of neuronal activity for brain development has been demonstrated by numerous studies that relied on sensory deprivation, pharmacological suppression of ion channels, or silencing of specific cell types (Chen et al., 2012; De Marco Garcia et al., 2011; Espinosa and Stryker, 2012; Hensch, 2005; Hubel and Wiesel, 1962; Huberman et al., 2006; Kerschensteiner et al., 2009; Kozorovitskiy et al., 2012; Lendvai et al., 2000; Liu et al., 2012; Lu et al., 2013; Maffei et al., 2006; Shatz and Stryker, 1988; Sretavan et al., 1988; van Versendaal et al., 2012; Wang et al., 2007; Wiesel and Hubel, 1963; Yu et al., 2004). While a given neuron can be excited by signals from multiple sources, structural plasticity of circuits in higher brain regions is predominantly driven by synaptic release of glutamate. Glutamatergic inputs regulate synapse numbers and properties of persistent synapses via mechanisms that involve transcription, local protein synthesis, trafficking, and posttranslational modifications (Anggono and Huganir, 2012; Citri and Malenka, 2008; Tom Dieck et al., 2014; West and Greenberg, 2011). However, several genetic experiments have also supported the notion that synapses do not need to be active to form. First, asymmetric contacts with vesicle pools have been found in cortices of Munc13 and Munc18 mouse mutants that completely lacked transmitter release in all neurons, albeit these mice could only be analyzed at birth, when connectivity in the forebrain is still rudimental (Varoqueaux et al., 2002; Verhage et al., 2000). Subsequently, exocytosis of neurotransmitter vesicles has been shown to be unnecessary for gross synaptic differentiation *in vitro* and in several neuron types *in vivo* (Deak et al., 2004; Harms and Craig, 2005; Imig et al., 2014; Lopez et al., 2012; Pieraut et al., 2014; Schoch et al., 2001; Shimojo et al., 2015; Yu et al., 2004; Zhang et al., 2008). Lastly, ionotropic glutamate receptors have been recently found to be dispensable for morphogenesis of dendritic trees and spines of pyramidal cells in the CA1 (Lu et al., 2013), although this conclusion was based on sparse gene knockouts, and the contribution of metabotropic receptor signaling could not be ruled out (Dore et al., 2016).

Here, we extend these observations by examining the morphologies, wiring, and ultra-structural organization of synapses of excitatory neurons in the postnatal hippocampus that developed in nearly complete absence of vesicular glutamate release. Our results highlight an instructive role of intrinsic programs in several key aspects of circuit and synapse formation.

## RESULTS

### Broad silencing of excitatory pathways in the developing forebrain

To study intrinsic assembly of excitatory synapses in circuits essential for learning and memory, we permanently suppressed vesicular release in glutamatergic neurons in the developing mouse forebrain. This was accomplished via Cre-inducible expression of Tetanus

toxin (TeNT), a protease that blocks the exocytosis of neurotransmitter vesicles by cleaving SNARE, Synaptobrevin/VAMP2 (Syb2) (Link et al., 1992; Schoch et al., 2001). We crossed the $R26^{floxstopTeNT}$ allele (Zhang et al., 2008) with $Emx1^{IRES\text{-}Cre}$, which drives recombination in progenitors that give rise to >95% of principal neurons in the dorsal telencephalon (Gorski et al., 2002) (Figures 1A, 1B and S1). Under these conditions, TeNT was broadly and irreversibly expressed starting from mid gestation, before synapses begin to form. While progenitors of the Emx1 lineage also generate glia (Gorski et al., 2002), we reasoned that cleavage of TeNT-sensitive SNAREs in astrocytes could alleviate compensatory effects of glutamate secreted from non-synaptic sources.

We confirmed a widespread loss of Syb2 in forebrains of neonatal offspring of $Emx1^{IRES\text{-}Cre}/R26^{floxstopTeNT}$ mice (which we refer to as Emx1/TeNT) by immunoblotting and immunofluorescent microscopy (Figures 1C and 1D). In the cerebral cortex and the hippocampus, the SNARE was absent in virtually all nascent synapses that recruited the vesicular glutamate transporter, VGlut1 (Figures 1E, 1F, S2A–C and data not shown).

Neurotransmitter vesicles contain up to 70 copies of Syb2, but their fusion with plasma membrane is catalyzed by as few as 3 ternary SNARE complexes (Mohrmann et al., 2010; Takamori et al., 2006). To address the concern that incompletely degraded Syb2 supports residual exocytosis, we first monitored neurotransmission in primary cultures. In agreement with earlier studies of Syb2-deficient neurons cultured *in vitro* (Deak et al., 2004; Harms and Craig, 2005; Schoch et al., 2001; Shimojo et al., 2015), neurons dissociated from cortices of Emx1/TeNT pups formed synapses but failed to generate evoked and spontaneous excitatory postsynaptic currents (EPSCs), indicating that release of glutamate was suppressed (Figures S2D–F and Table S1).

Unlike previously described mutants that lacked essential secretory proteins in the entire nervous system (Schoch et al., 2001; Varoqueaux et al., 2002; Verhage et al., 2000), Emx1/TeNT mice could survive for weeks (see Methods). These animals had markedly reduced body weights and exhibited aberrant behavior in the standard laboratory environment. However, their brains were only slightly smaller and had undistorted anatomies with appropriate lamination of cellular layers, no apparent increase in apoptosis, and preserved expression of many synaptic proteins (Figures 1G–I, S3A–I; Movies S1 and S2). To ensure that Emx1-driven TeNT irreversibly blocks synaptic transmission early in development, we sampled EPSCs from CA1 pyramidal cells in acute slices. No evoked AMPA- and NMDA currents could be detected in the CA1 of Emx1/TeNT mice at p3 and p30, even when the Schaffer collateral path was stimulated at high frequency. Spontaneous vesicle fusion events were negligible in the normal CA1 at p3, yet, recordings from older animals showed that miniature neurotransmission was also abolished by TeNT (Figures 1J–L and Table S1). These results validate the Emx1/TeNT mouse model for analysis of synaptic connectivity in circuits comprised of release-deficient glutamatergic neurons.

## Presynaptic differentiation of excitatory neurons in the hippocampus

Despite widespread expression of TeNT, the cerebral cortex of Emx1/TeNT mice may be excited by thalamic afferents (Viaene et al., 2011). Indeed, staining for VGlut2, which is enriched in terminals of thalamic axons (Bopp et al., 2017), and recordings of EPSCs from

layer IV of the somatosensory cortex suggested that thalamic inputs onto Syb2-deficient cortical neurons formed (Figure S3J and Table S1). We therefore primarily focused on the hippocampus, which is comprised of and largely innervated by glutamatergic neurons of the Emx1 lineage (Gorski et al., 2002). All subsequent studies were performed at postnatal week 4, when *de novo* synaptogenesis normally reaches a plateau and experience-dependent refinement of connectivity is nearly complete (Espinosa and Stryker, 2012).

The main excitatory hippocampal trisynaptic pathway relays information from the entorhinal cortex (EC) to the DG and areas CA3/CA1 (Forster et al., 2006). To determine how this pathway assembles in Emx1/TeNT mice, we examined long-range projections and presynaptic boutons using immunohistochemistry and viral tracing. Neither approach revealed defects in lamination of the hippocampus. The appropriate targeting of entorhinal axons and granule cell (GC) mossy fibers was particularly evident when these projections were selectively tagged with membrane-bound GFP, expressed in a Cre-inducible manner from an AAV (AAVDJ DIO-mGFP) (Figures 2A–D and S5A–G). Staining for VGlut1 and a GC-enriched presynaptic protein, Synaptoporin (SPO) (Pieraut et al., 2014; Williams et al., 2011), showed that axons of release-deficient neurons formed abundant connections whose distribution across different axes also appeared normal (Figures 2E–G). These observations were not merely attributed to inefficient cleavage of Syb2 and/or silencing of release. Just like newborn Emx1/TeNT pups, 4 weeks old animals lacked Syb2 in virtually all boutons containing SPO and VGlut1. The remaining Syb2 puncta colocalized with synapses of spared GABAergic interneurons that recruit VGAT (Figures 2F–H and S4). Furthermore, recordings of EPSCs from CA3 pyramidal cells and dentate GCs in acute slices confirmed that glutamatergic neurotransmission was suppressed throughout the pathway (Table S1).

While broad silencing did not perturb the overall organization of excitatory circuits, synapse numbers were affected to different extents in specific hippocampal subfields. We detected a ~30–50% decrease in the density of VGlut1 puncta in striatum radiatum of CA3/CA1 and striatum oriens of the CA3 with no significant changes in the molecular layer of the DG and stratum lucidum of the CA3 (Figure 2I). The total numbers of SPO-positive large mossy fiber terminals (LMTs) as well as their linear densities along individual axons were also unaffected (Figure S5D).

## Postsynaptic differentiation of excitatory neurons

To explore how these changes, or lack thereof, in wiring of the hippocampus correlate with postsynaptic differentiation of projection neurons, we inspected the dendrites and spines of single cells that were tagged with AAVDJ DIO-mGFP. Mice were injected to achieve sparse expression of the reporter in the CA1 or DG, neurons were imaged at p30, and their morphologies were reconstructed from 3D stacks (Figures 3A and 3B). Both pyramidal cells and dentate GCs of Emx1/TeNT mutants possessed fully polarized dendrites. However, arborization was significantly reduced in the CA1, but not in the DG, mainly at the expense of branch tips (Figures 3C–E). Likewise, both neuron subtypes had abundant spines, but linear spine densities were reduced by ~40% in the CA1, consistent with counts of VGlut1-positive presynaptic boutons (Figures 3F and 3G). Curiously, tracing pyramidal cells in superficial layers of the somatosensory cortex revealed morphological defects that were

nearly identical to CA1 (Figures S5H–K). The latter implies that thalamic excitation alone cannot fully support the development of cortical circuits.

Considering that dendritic protrusions have heterogeneous shapes and their growth may be affected by network activity (Bourne and Harris, 2012; Holtmaat and Svoboda, 2009; Sudhof and Malenka, 2008), we assessed the distributions of morphologically distinct spines. Loss of neurotransmission did not prevent the formation of common spine types, including mushroom spines that recruit new glutamate receptors during long-term potentiation (LTP) and learning (Makino and Malinow, 2011; Malenka and Bear, 2004; Matsuo et al., 2008). The fractions of mushroom spines remained unchanged in all examined areas, despite nonuniform effects of synaptic activity deprivation on total terminal/spine numbers (Figures 3G and S5L).

Because we were unable to achieve reliable viral infection in the CA3, we interrogated proximal dendrites of pyramidal cells in this region by serial block-face scanning electron microscopy (SBEM). 3D reconstruction analysis demonstrated that complex spines, whose structures likely reflect the sizes and complexity of presynaptic LMTs, also formed in stratum lucidum of Emx1/TeNT mice (Figure 3H). In fact, release-deficient CA3 neurons had a ~30% increase in spine density, and their volumes and surfaces areas were significantly larger (Figure 3I).

## Architectures of single glutamatergic synapses

Our results highlight a limited role of glutamatergic neurotransmission in development of connectivity between projection neurons in the hippocampal pathway. Furthermore, the counterintuitive preservation of spinogenesis in the absence of vesicular release raises the possibility that permanently silenced, intrinsically formed, synapses are structurally mature. We tested this hypothesis by using serial electron microscopy (SEM). Tomographic images were acquired from 300 nm sections, and terminals with opposed spines that contain characteristic postsynaptic densities (PSDs) were reconstructed for 3D view from serial stacks.

Previous studies have shown that, in cultured neurons from Syb2 knockout mice, synaptic vesicles have irregular shapes (Deak et al., 2004). This abnormality could be attributed to prolonged lifetime of trafficking organelles due to lack of recycling, or alternatively, distortion of protein networks on a vesicle surface. We found that *in vivo* expression of TeNT also affects vesicle volumes and spherisity, permitting identification of release-deficient synapses with nearly a 100% accuracy in samples of undisclosed genotypes (Figures 4B, 4C and S6). We thus collected 3D image sets from stratum radiatum of the CA1, molecular layer of the DG and layer III of primary somatosensory cortex where terminals of cortical neurons carrying TeNT could be easily distinguished from intact terminals of thalamic axons.

Similar to lower-resolution SBEM imaging of uncommonly branched spines on CA3 neuron dendrites (Figure 3H), SEM showed that conventional excitatory synapses were larger in all three brain regions of Emx1/TeNT mice. Yet, these synapses resembled connections in the normal brain with terminals containing docked and reserved vesicle pools, defined clefts,

and well-developed PSDs (Figures 4D and S6). Moreover, the increase in synapse sizes was not due to asymmetrical swelling of particular structures. Rather, we detected a proportional expansion of presynaptic boutons, spines, and PSDs with no differences in densities of vesicles tethered to active zones and volumes of PSDs relative to total spine volumes (Figures 4D, 4E and Table S2).

## DISCUSSION

We have shown that projection neurons in the hippocampus differentiate, develop stereotyped connectivity, and form structurally mature synapses independently of vesicular release of glutamate. Our work extends the earlier findings that global inactivation of synaptic vesicle exocytosis does not preclude synaptogenesis *in vitro* and in the embryonic brain, as well as the recent study of cell-autonomous functions of ionotropic glutamate receptors in the CA1 (Deak et al., 2004; Harms and Craig, 2005; Imig et al., 2014; Lu et al., 2013; Schoch et al., 2001; Shimojo et al., 2015; Varoqueaux et al., 2002; Verhage et al., 2000). Taken together, these experiments highlight the key role of intrinsic genetic programs in circuit and synapse assembly.

Tetanus toxin has been previously used for presynaptic silencing in several parts of the nervous system including spinal cord, retina, olfactory epithelium, cerebral cortex, and the hippocampus (Kerschensteiner et al., 2009; Lopez et al., 2012; Okawa et al., 2014; Pieraut et al., 2014; Wang et al., 2007; Yu et al., 2004; Zhang et al., 2008). Some of these studies have supported the model that neurotransmission is essential for refinement of connectivity in a competitive environment; however, silencing had different outcomes in different circuits. For instance, targeted expression of TeNT interfered with synapse formation in retinal bipolar cells, disrupted arborization of callosal axons in the somatosensory cortex, but had no apparent effect on GC mossy fibers (Kerschensteiner et al., 2009; Lopez et al., 2012; Pieraut et al., 2014; Wang et al., 2007). Though activity-dependent competition in the hippocampus of Emx1/TeNT mice is unlikely, our results also exemplify how capacities for hardwiring differ among diverse neuron types. The non-uniform changes in dendrite morphologies and synapse numbers across hippocampal axes may be attributed to cell-specific mechanisms that stabilize nascent contacts formed during experience and learning, or promote pruning (Holtmaat and Svoboda, 2009; Mikuni et al., 2013; Moser et al., 1994; Trachtenberg et al., 2002; Tsai et al., 2012; Wiegert and Oertner, 2013; Xu et al., 2009). While dentate GCs appear to be especially tolerant to loss of glutamatergic input/output, fine-scale miswiring of their connections could still occur. In addition, DG-dependent tasks require gradual integration of adult-born neurons (Aimone et al., 2014; Nakashiba et al., 2012), which has not been examined herein.

Suppressing all signals that elicit neuronal activity in a whole animal is technically challenging. It is conceivable that, at a circuit level, the phenotypes of Emx1/TeNT mice are partially attributed to compensatory mechanisms that augment intrinsic excitability of glutamatergic neurons and/or mediate calcium influx in response to extrinsic cues from non-synaptic sources. Indeed, spontaneous wave-like activities have been shown to play critical roles during initial stages of circuit formation (Espinosa and Stryker, 2012; Katz and Shatz, 1996; Shatz and Stryker, 1988). Also, GABA is thought to act as a depolarizing

neurotransmitter early in development (Khakhalin, 2011) and, although synaptic strengths of GABAergic interneurons is generally proportional to excitation (Isaacson and Scanziani, 2011), the contribution of spontaneous GABA release cannot be ruled out. Nonetheless, we can conclude that vesicular release of glutamate per se is unnecessary for morphogenesis and maintenance of individual nerve terminals and dendritic spines. The ability of principal neurons to form mushroom spines and pronounced PSDs without presynaptic input is particularly noteworthy, considering that sensory experience and glutamate-induced excitation affect the numbers and architectures of spines *in vitro* and *in vivo* (Alvarez and Sabatini, 2007; Anggono and Huganir, 2012; Colgan and Yasuda, 2014; Collin et al., 1997; Gomperts et al., 2000; Holtmaat and Svoboda, 2009; Holtmaat et al., 2006; Kwon and Sabatini, 2011; Matsuo et al., 2008; McKinney et al., 1999; Moser et al., 1994; Richards et al., 2005). Moreover, synaptic excitation promotes the SNARE-dependent exocytosis of peptidergic vesicles that secrete trophic factors implicated in spine plasticity, such as BDNF (Harward et al., 2016; Matsuda et al., 2009; Park et al., 2014; Shimojo et al., 2015). The proportional increase in terminal/spine volumes in our mouse model is reminiscent of heterogeneity of synapse sizes in the normal brain, and can be explained by lack of membrane recycling or homeostatic response, since transient changes in synaptic strength produce opposite effects: spines shrink with LTD and expand during LTP and associative learning (Bourne and Harris, 2011; Holtmaat and Svoboda, 2009; Ostroff et al., 2010; Ramiro-Cortes and Israely, 2013; Sudhof and Malenka, 2008; Zhou et al., 2004).

Synaptogenesis is orchestrated by secreted, transmembrane and intracellular proteins that guide axons to receptive fields, mediate surface adhesion, and recruit numerous molecules to active zones and opposed postsynaptic sites (Kolodkin and Tessier-Lavigne, 2011; Krueger et al., 2012; Shen and Scheiffele, 2010; Sudhof, 2012; Tada and Sheng, 2006). Although these molecules can be regulated by excitatory neurotransmission at many levels and the contribution of experience to structural plasticity has been proven beyond any doubt, our results imply that assembly of basic building blocks of glutamatergic synapses is controlled by developmental programs that do not require transmitter release and subsequent activation of postsynaptic receptors.

## STAR METHODS

### CONTACT FOR REAGENTS AND RESOURCE SHARING

Further information and requests for resources and reagents should be directed to and will be fulfilled by the Lead Contact, Anton Maximov (amaximov@scripps.edu)

### EXPERIMENTAL MODEL AND SUBJECT DETAILS

**Mice—***Emx1*$^{IRES\text{-}Cre}$, *Ai9* tdTomato Cre reporter, and *R26*$^{floxstopTeNT}$ alleles were described previously (Gorski et al., 2002; Madisen et al., 2010; Zhang et al., 2008). Mice carrying these alleles were mated to produce conditional lines, housed, and analyzed according to protocols approved by the Institutional Animal Care and Use Committee. Stains were maintained in mixed C56BL/6 and 129/Sv backgrounds. In all experiments, *R26*$^{floxstopTeNT}$/*Emx1*$^{IRES\text{-}Cre}$ mutants (heterozygous for each allele) and their control TeNT-negative littermates were examined in parallel. Studies were performed with animals

of both sexes. Ages are indicated in the main text and figure legends. Housing conditions are described in method details.

**Cell culture—**Neurons and glia were isolated from the cortices of p1 pups of both sexes. The cells were dissociated by trypsin digestion and plated on circle glass coverslips (Carolina Biological Supply) coated with Matrigel (Collaborative Biochemical Product, Inc). Primary cultures were maintained at 37C in MEM (Invitrogen) supplemented with B-27 (Invitrogen), glucose, transferrin and Ara-C (Sigma). Recombinant adeno-associated viruses were produced in HEK293 cells (ATCC) that were maintained at 37C in MEM and fetal bovine serum.

## METHOD DETAILS

**Mice—**Newborn Emx1/TeNT pups suckled but were unable to survive for more than 2–3 days in standard housing environment, perhaps due to competition with normal littermates for mother's milk and, subsequently, inability to find solid food and water. To alleviate this problem, we kept Emx1/TeNT mice with mothers until experiments and placed food and gels with water directly on cage floors for easy access. Under these conditions, Emx1/TeNT mice could survive for weeks, albeit at a much lower than expected Mendelian ratio. We assume that progressive delay in body growth is associated with abnormal metabolism rather than food intake, but the exact mechanisms are unclear. We also noted that survival of Emx1/TeNT mice is background dependent: we were unable to obtain any offspring older that 2–3 days from crosses of $R26^{floxstopTeNT}$ and $Emx1^{IRES\text{-}Cre}$ founders of a pure C56BL/6 background.

**Electrophysiology—**Spontaneous and evoked synaptic currents were monitored in whole-cell voltage clamp mode using a Multiclamp 700B amplifier (Molecular Devices, Inc.). Evoked release was triggered by 1 ms current injections trough the local extracellular stimulating electrode (FHC, Inc. CBAEC75). The frequency, duration, and magnitude of extracellular stimuli were controlled by Model 2100 Isolated Pulse Stimulator (A-M Systems, Inc.). Currents were sampled at 10 kHz and analyzed offline with pClamp10 (Molecular Devices, Inc.) and Origin8 (Origin Lab) software packages. For recording from cultured neurons, the whole-cell pipette solution contained 135 mM $CsCl_2$, 10 mM HEPES-NaOH pH 7.4, 1 mM EGTA, 1 mM Na-ATP, 0.4 mM Na-GTP, and 1 mM QX-314. The resistance of filled pipettes varied between 3–5 mOhm. The bath solution contained 140 mM NaCl, 5 mM KCl, 2 mM $CaCl_2$, 0.8 mM $MgCl_2$, 10 mM HEPES-NaOH pH 7.4, and 10 mM glucose. eEPSCs and eIPSCs were separated pharmacologically by addition of 100 μM picrotoxin or 50 μM APV and 10 μM CNQX, respectively, to the bath solution. sEPSCs were monitored in the presence of 1 μM tetrodotoxin.

For acute slice physiology, mice were anesthetized with isoflurane and the brains were removed and placed into ice-cold oxygenated 95%$O_2$/5%$CO_2$ buffer containing 110 mM Sucrose, 87 mM NaCl, 2.5 mM KCl, 0.5 mM $CaCl_2$, 7 mM $MgCl_2$, 25 mM $NaHCO_3$, 1.25 mM $NaH_2PO_4$ and 20 mM Glucose. Transverse, 350 μm thick slices were cut with a vibratome and initially stored at 32°C in oxygenated artificial cerebrospinal fluid (ACSF) containing 125 mM NaCl, 2.5 mM KCl, 2 mM $NaH_2PO_4$, 25 mM $NaHCO_3$, 1.3 mM

$MgCl_2$, 2 mM $CaCl_2$, 10 mM Glucose, pH 7.4. Slices were then allowed to recover for ~1 hour in oxygenated 95%$O_2$/5%$CO_2$ ACSF at 24°C prior to recording. The whole-cell recordings were performed at room temperature. The whole-cell pipette solution contained 122.5 mM $C_6H_{12}O_7$, 122.5 mM CsOH, 10 mM CsCl, 1.5 mM $MgCl_2$, 5 mM NaCl, 1 mM EGTA, 5 mM HEPES, 3 mM MgATP, 0.3 mM NaGTP, 5 mM QX-314, and 10 mM $Na_2$phosphocreatine (pH 7.4, adjusted with CsOH to 280–290 mOsm). EPSCs and IPSCs were separated pharmacologically, as described above. eEPSCs were sampled from mature granule cells in the upper GCL of the DG and pyramidal neurons in the CA3 and CA1 following local extracellular stimulation of the perforant path, mossy fibers and schaffer collateral axons, respectively. For recordings from cortical neurons, evoked responses were triggered by placing an electrode near dendritic fields of cells with attached pipettes. For all areas, input-output relationships were determined in slices from wildtype mice to prevent failures. To further minimize the variance, eEPSC amplitudes were calculated for each cell after averaging 5–10 responses that were collected during repetitive low-frequency stimulation at 0.1 Hz.

**Virus production and injection—**Adeno-associated viruses (AAVs) were produced with shuttle vectors containing inverted terminal repeats, the WPRE element, and the hGH polyadenylation signal. To achieve cell type-specific, Cre-inducible expression of fluorescent reporters, coding sequences were flanked by two pairs of loxP sites (DIO) and inserted downstream of a 1.26 kb EF1α promoter in a 3′-5′ orientation. These vectors were packed in house into AAV serotype DJ using published protocols (McClure et al., 2011). p3 pups were injected with 0.5μl of viral stocks via glass micropipettes (10 μm tip diameter) and returned to home cages until experiments (p30). Recombination was driven with *Emx1*$^{IRES\text{-}Cre}$ or, in some cases, previously characterized AAV2.2 Syn:Cre that was co-injected with tracer viruses (Pieraut et al., 2014). For analysis of entorhinal axons and mossy fibers, undiluted viruses ($5 \times 10^{11} – 10^{12}$ GC/ml) were injected into cerebral lateral ventricles and ENT layers II/III, respectively. Appropriate targeting was confirmed by imaging GFP-positive cell bodies, and a consistent infection density across animals was confirmed by calculating the ratio of GFP-labeled cells to DAPI. For reconstruction of dendritic trees, stocks were diluted to achieve sparse labeling of principal neurons in the cortex, DG and CA1. The targeting specificity was confirmed by staining with antibodies to excitatory neuron-specific markers. Stellate cells were excluded from analyses of neuronal morphologies in superficial cortical layers. In the DG, we exclusively analyzed fully differentiated GCs that reside in the upper granule cells layer.

**Immunohistochemistry—**Mice were anesthetized with isofluorane and perfused with 4% PFA. The brains were incubated overnight in 0.5% PFA, and sliced on vibratome in ice cold PBS. The 90 μm thick, free-floating coronal sections (Bregma −1.4 to −2.5) were briefly boiled in 0.1 M citrate buffer for antigen retrieval. Sections were then washed 3 times in PBS, blocked for 1 hour in 4% BSA, 3% donkey serum, 0.1% Triton, and incubated overnight with primary antibodies diluted in blocking solution, followed by brief washes in PBS and 3 hour incubation with corresponding fluorescently labeled secondary antibodies. Samples were washed again and mounted on glass slides.

**Acquisition and analysis of confocal images—**Specific brain regions were annotated using Allen Brain Atlas as a reference (http://mouse.brain-map.org/static/atlas). Images were collected under the Nikon C2 confocal microscope with 10×, 20× and 40× or 60× objectives. Thresholds and laser intensities were established for individual channels and equally applied to the entire dataset. Conventional image analysis was conducted with Nikon Elements, FIJI, and Adobe Photoshop software packages. Digital manipulations were equally applied to all pixels. For binning analysis of immunolabeled synapses, grids were constructed in FIJI at 10 μm intervals and puncta was counted in each bin. 3D images of dendritic trees of single virally-labeled neurons were collected from 200 μm coronal sections at 0.2 μm Z intervals. Neurons were subsequently reconstructed from serial stacks and analyzed in Neurolucida, as we have previously described (Pieraut et al., 2014).

**Electron microscopy—**Mice were transcardially perfused with Ringer's solution followed by perfusion with 150 mM cacodylate, 2.5% glutaraldehyde, 2% paraformaldehyde and 2 mM $CaCl_2$. The brains were fixed overnight in the same buffer at 4 °C and cut into 100 μm coronal sections on vibratome. The slices were fixed overnight at 4 °C and then washed for 1 hour in 150 mM cacodylate/2 mM $CaCl_2$ on ice. 300 nm thick sections were cut from the SBEM-stained specimens and collected on 50 nm Luxel slot grids (Luxel Corp., Friday Harbor, WA). The grids were coated with 10 nm colloidal gold (Ted Pella, Redding, CA) and imaged at 300 keV on a Titan TEM (FEI, Hillsboro, OR). Double-tilt tilt-series were collected with 0.5 degree tilt increments at 22,500X magnification on a 4k × 4k Gatan Ultrascan camera. Tomograms were generated with an iterative scheme in the TxBR package (Chen et al., 2014). Segmentation of synaptic structures and vesicle pools were performed in IMOD. For analysis of vesicle volumes and shapes, histograms were fitted with the following functions in Origin8: Gaussian: y=y0+(A/(w*sqrt(PI/2)))*exp(-2*((x-xc)/w)^2); Asym2Sig: y=y0+A*(1/(1+exp(-(x-xc+w1/2)/w2)))*(1-1/(1+exp(-(x-xc-w1/2)/w3))).

## QUANTIFICATION AND STATISTICAL ANALYSIS

Means and standard errors were calculated in Origin8. *P* values were determined with Student's *t*-test. Quantifications of dendrite morphologies, synapse densities, and EM analyses of synapse structure were performed in a "blind" manner by investigators who were unaware of genotypes. Details, including sample sizes, can be found in figure legends.

KEY RESOURCES TABLE

| REAGENT or RESOURCE | SOURCE | IDENTIFIER |
|---|---|---|
| Antibodies | | |
| NeuN | Millipore | Cat#MAB377, RRID: AB_2298772 |
| Cux1 | Santa Cruz | Cat#SC-13024, RRID:AB_2261231 |
| Ctip2 | Abcam | Cat#AB18465, RRID:AB_2064130 |
| Tbr1 | Abcam | Cat#AB31940, RRID:AB_2200219 |
| Cleaved caspase-3 | Cell Signaling | Cat#9661, RRID:AB_2341188 |
| VGlut1 | Synaptic Systems | Cat#135303, RRID:AB_887875 |

| REAGENT or RESOURCE | SOURCE | IDENTIFIER |
|---|---|---|
| Calbindin D-28k | Swant | Cat#CB38, RRID:AB_10000340 |
| GFP | AVES | Cat#GFP1010, RRID:AB_2307313 |
| GFAP | Millipore | Cat#MAB360, RRID:AB_2109815 |
| Tuj1 | Sigma | Cat#T2200, RRID:AB_262133 |
| NR1 | Synaptic Systems | Cat#114011, RRID:AB_887750 |
| NR2A | Invitrogen | Cat#32-0600, RRID:AB_86918 |
| GluR1 | Millipore | Cat#AB1504, RRID:AB_2113602 |
| GABAar | Millipore | Cat#06-868, RRID:AB_310272 |
| Syb2 | Synaptic Systems | Cat#104211C3, RRID:AB_887808 |
| Synaptoporin (SPO) | Synaptic Systems | Cat#102002, RRID:AB_887841 |
| c-Fos | Millipore | Cat#PC38, RRID:AB_2106755 |
| VGAT | Synaptic Systems | Cat#131003, RRID:AB_887869 |
| Vglut2 | Synaptic Systems | Cat#135421, RRID:AB_2619823 |
| All other antibodies were homemade and were a kind gift from Dr. Thomas C. Südhof | | |
| Bacterial and Virus Strains | | |
| AAVDJ DIO-mGFP | Maximov lab | Pieraut et al., PMID: 25277456 |
| AAV2.2 Syn:Cre | Maximov lab | Pieraut et al., PMID: 25277456 |
| Chemicals, Peptides, and Recombinant Proteins | | |
| APV | Tocris | Cat#01061 |
| CNQX | Tocris | Cat#01045 |
| Picrotoxin | Tocris | Cat#1128 |
| Tetrodotoxin | Tocris | Cat#4368289 |
| Experimental Models: Cell Lines | | |
| HEK293t | ATCC | |
| Primary neuronal cultures | This paper | |
| Experimental Models: Organisms/Strains | | |
| Emx1$^{IRES\text{-}Cre}$ mouse allele | JAX | Gorski et al., PMID: 12151506 |
| Ai9 Cre reporter mouse allele | JAX | Madisen et al., PMID:20023653 |
| *R26$^{floxstopTeNT\ mouse\ allele}$* | Dr. Martyn Goulding | Zhang el al., PMID:18940590 |
| Software and Algorithms | | |
| pCamp10 | Molecular Devices | |
| Origin8 | Origin Lab | |
| Nikon Elements | Nikon | |
| Neurolucida | MBF Bioscience | |
| FIJI | ImageJ | |

## Supplementary Material

Refer to Web version on PubMed Central for supplementary material.

## Acknowledgments

We thank Drs. T. C. Südhof, A. Patapoutian, L. Stowers, M. Mayford, F. Polleux, and S. Leutgeb for discussions and critical comments; Drs. M. Goulding and F. Polleux for sharing mice; Dr. K. Spencer for assistance with microscopy; and R. Koch for editing the manuscript. This study was supported by NIH grants R01MH085776 (to A.M.), R01NS087026 (A.M.), P41GM103412 (M.E.), NS027177I (M.E.), DA038896 (M.E.) and F31MH094059 (R.S.).

## References

Aimone JB, Li Y, Lee SW, Clemenson GD, Deng W, Gage FH. Regulation and function of adult neurogenesis: from genes to cognition. Physiological reviews. 2014; 94:991–1026. [PubMed: 25287858]

Alvarez VA, Sabatini BL. Anatomical and physiological plasticity of dendritic spines. Annual review of neuroscience. 2007; 30:79–97.

Anggono V, Huganir RL. Regulation of AMPA receptor trafficking and synaptic plasticity. Current opinion in neurobiology. 2012; 22:461–469. [PubMed: 22217700]

Bopp R, Holler-Rickauer S, Martin KA, Schuhknecht GF. An ultrastructural study of the thalamic input to layer 4 of primary motor and primary somatosensory cortex in the mouse. The Journal of neuroscience : the official journal of the Society for Neuroscience. 2017

Bourne JN, Harris KM. Coordination of size and number of excitatory and inhibitory synapses results in a balanced structural plasticity along mature hippocampal CA1 dendrites during LTP. Hippocampus. 2011; 21:354–373. [PubMed: 20101601]

Bourne JN, Harris KM. Nanoscale analysis of structural synaptic plasticity. Current opinion in neurobiology. 2012; 22:372–382. [PubMed: 22088391]

Chen JL, Villa KL, Cha JW, So PT, Kubota Y, Nedivi E. Clustered dynamics of inhibitory synapses and dendritic spines in the adult neocortex. Neuron. 2012; 74:361–373. [PubMed: 22542188]

Chen R, Wan X, Altintas I, Wang J, Crawl D, Phan S, Lawrence A, Ellisman M. EPiK-a Workflow for Electron Tomography in Kepler. Procedia computer science. 2014; 20:2295–2305. [PubMed: 25621086]

Citri A, Malenka RC. Synaptic plasticity: multiple forms, functions, and mechanisms. Neuropsychopharmacology : official publication of the American College of Neuropsychopharmacology. 2008; 33:18–41. [PubMed: 17728696]

Colgan LA, Yasuda R. Plasticity of dendritic spines: subcompartmentalization of signaling. Annual review of physiology. 2014; 76:365–385.

Collin C, Miyaguchi K, Segal M. Dendritic spine density and LTP induction in cultured hippocampal slices. Journal of neurophysiology. 1997; 77:1614–1623. [PubMed: 9084624]

De Marco Garcia NV, Karayannis T, Fishell G. Neuronal activity is required for the development of specific cortical interneuron subtypes. Nature. 2011; 472:351–355. [PubMed: 21460837]

Deak F, Schoch S, Liu X, Sudhof TC, Kavalali ET. Synaptobrevin is essential for fast synaptic-vesicle endocytosis. Nature cell biology. 2004; 6:1102–1108. [PubMed: 15475946]

Dore K, Aow J, Malinow R. The Emergence of NMDA Receptor Metabotropic Function: Insights from Imaging. Frontiers in synaptic neuroscience. 2016; 8:20. [PubMed: 27516738]

Espinosa JS, Stryker MP. Development and plasticity of the primary visual cortex. Neuron. 2012; 75:230–249. [PubMed: 22841309]

Forster E, Zhao S, Frotscher M. Laminating the hippocampus. Nature reviews Neuroscience. 2006; 7:259–267. [PubMed: 16543914]

Gomperts SN, Carroll R, Malenka RC, Nicoll RA. Distinct roles for ionotropic and metabotropic glutamate receptors in the maturation of excitatory synapses. The Journal of neuroscience : the official journal of the Society for Neuroscience. 2000; 20:2229–2237. [PubMed: 10704498]

Gorski JA, Talley T, Qiu M, Puelles L, Rubenstein JL, Jones KR. Cortical excitatory neurons and glia, but not GABAergic neurons, are produced in the Emx1-expressing lineage. The Journal of neuroscience : the official journal of the Society for Neuroscience. 2002; 22:6309–6314. [PubMed: 12151506]

Harms KJ, Craig AM. Synapse composition and organization following chronic activity blockade in cultured hippocampal neurons. The Journal of comparative neurology. 2005; 490:72–84. [PubMed: 16041714]

Harward SC, Hedrick NG, Hall CE, Parra-Bueno P, Milner TA, Pan E, Laviv T, Hempstead BL, Yasuda R, McNamara JO. Autocrine BDNF-TrkB signalling within a single dendritic spine. Nature. 2016; 538:99–103. [PubMed: 27680698]

Hensch TK. Critical period plasticity in local cortical circuits. Nature reviews Neuroscience. 2005; 6:877–888. [PubMed: 16261181]

Holtmaat A, Svoboda K. Experience-dependent structural synaptic plasticity in the mammalian brain. Nature reviews Neuroscience. 2009; 10:647–658. [PubMed: 19693029]

Holtmaat A, Wilbrecht L, Knott GW, Welker E, Svoboda K. Experience-dependent and celltype-specific spine growth in the neocortex. Nature. 2006; 441:979–983. [PubMed: 16791195]

Hubel DH, Wiesel TN. Receptive fields, binocular interaction and functional architecture in the cat's visual cortex. The Journal of physiology. 1962; 160:106–154. [PubMed: 14449617]

Huberman AD, Speer CM, Chapman B. Spontaneous retinal activity mediates development of ocular dominance columns and binocular receptive fields in v1. Neuron. 2006; 52:247–254. [PubMed: 17046688]

Imig C, Min SW, Krinner S, Arancillo M, Rosenmund C, Sudhof TC, Rhee J, Brose N, Cooper BH. The morphological and molecular nature of synaptic vesicle priming at presynaptic active zones. Neuron. 2014; 84:416–431. [PubMed: 25374362]

Isaacson JS, Scanziani M. How inhibition shapes cortical activity. Neuron. 2011; 72:231–243. [PubMed: 22017986]

Katz LC, Shatz CJ. Synaptic activity and the construction of cortical circuits. Science. 1996; 274:1133–1138. [PubMed: 8895456]

Kerschensteiner D, Morgan JL, Parker ED, Lewis RM, Wong RO. Neurotransmission selectively regulates synapse formation in parallel circuits in vivo. Nature. 2009; 460:1016–1020. [PubMed: 19693082]

Khakhalin AS. Questioning the depolarizing effects of GABA during early brain development. Journal of neurophysiology. 2011; 106:1065–1067. [PubMed: 21593390]

Kimchi T, Xu J, Dulac C. A functional circuit underlying male sexual behaviour in the female mouse brain. Nature. 2007; 448:1009–1014. [PubMed: 17676034]

Kolodkin AL, Tessier-Lavigne M. Mechanisms and molecules of neuronal wiring: a primer. Cold Spring Harbor perspectives in biology. 2011:3.

Kozorovitskiy Y, Saunders A, Johnson CA, Lowell BB, Sabatini BL. Recurrent network activity drives striatal synaptogenesis. Nature. 2012; 485:646–650. [PubMed: 22660328]

Krueger DD, Tuffy LP, Papadopoulos T, Brose N. The role of neurexins and neuroligins in the formation, maturation, and function of vertebrate synapses. Current opinion in neurobiology. 2012; 22:412–422. [PubMed: 22424845]

Kwon HB, Sabatini BL. Glutamate induces de novo growth of functional spines in developing cortex. Nature. 2011; 474:100–104. [PubMed: 21552280]

Lendvai B, Stern EA, Chen B, Svoboda K. Experience-dependent plasticity of dendritic spines in the developing rat barrel cortex in vivo. Nature. 2000; 404:876–881. [PubMed: 10786794]

Link E, Edelmann L, Chou JH, Binz T, Yamasaki S, Eisel U, Baumert M, Sudhof TC, Niemann H, Jahn R. Tetanus toxin action: inhibition of neurotransmitter release linked to synaptobrevin proteolysis. Biochemical and biophysical research communications. 1992; 189:1017–1023. [PubMed: 1361727]

Liu X, Ramirez S, Pang PT, Puryear CB, Govindarajan A, Deisseroth K, Tonegawa S. Optogenetic stimulation of a hippocampal engram activates fear memory recall. Nature. 2012; 484:381–385. [PubMed: 22441246]

Lopez CM, Pelkey KA, Chittajallu R, Nakashiba T, Toth K, Tonegawa S, McBain CJ. Competition from newborn granule cells does not drive axonal retraction of silenced old granule cells in the adult hippocampus. Frontiers in neural circuits. 2012; 6:85. [PubMed: 23162435]

Lu W, Bushong EA, Shih TP, Ellisman MH, Nicoll RA. The cell-autonomous role of excitatory synaptic transmission in the regulation of neuronal structure and function. Neuron. 2013; 78:433–439. [PubMed: 23664612]

Madisen L, Zwingman TA, Sunkin SM, Oh SW, Zariwala HA, Gu H, Ng LL, Palmiter RD, Hawrylycz MJ, Jones AR, et al. A robust and high-throughput Cre reporting and characterization system for the whole mouse brain. Nature neuroscience. 2010; 13:133–140. [PubMed: 20023653]

Maffei A, Nataraj K, Nelson SB, Turrigiano GG. Potentiation of cortical inhibition by visual deprivation. Nature. 2006; 443:81–84. [PubMed: 16929304]

Makino H, Malinow R. Compartmentalized versus global synaptic plasticity on dendrites controlled by experience. Neuron. 2011; 72:1001–1011. [PubMed: 22196335]

Malenka RC, Bear MF. LTP and LTD: an embarrassment of riches. Neuron. 2004; 44:5–21. [PubMed: 15450156]

Matsuda N, Lu H, Fukata Y, Noritake J, Gao H, Mukherjee S, Nemoto T, Fukata M, Poo MM. Differential activity-dependent secretion of brain-derived neurotrophic factor from axon and dendrite. The Journal of neuroscience : the official journal of the Society for Neuroscience. 2009; 29:14185–14198. [PubMed: 19906967]

Matsuo N, Reijmers L, Mayford M. Spine-type-specific recruitment of newly synthesized AMPA receptors with learning. Science. 2008; 319:1104–1107. [PubMed: 18292343]

McClure C, Cole KL, Wulff P, Klugmann M, Murray AJ. Production and titering of recombinant adeno-associated viral vectors. Journal of visualized experiments : JoVE. 2011:e3348. [PubMed: 22143312]

McKinney RA, Capogna M, Durr R, Gahwiler BH, Thompson SM. Miniature synaptic events maintain dendritic spines via AMPA receptor activation. Nature neuroscience. 1999; 2:44–49. [PubMed: 10195179]

Mikuni T, Uesaka N, Okuno H, Hirai H, Deisseroth K, Bito H, Kano M. Arc/Arg3.1 is a postsynaptic mediator of activity-dependent synapse elimination in the developing cerebellum. Neuron. 2013; 78:1024–1035. [PubMed: 23791196]

Mohrmann R, de Wit H, Verhage M, Neher E, Sorensen JB. Fast vesicle fusion in living cells requires at least three SNARE complexes. Science. 2010; 330:502–505. [PubMed: 20847232]

Moser MB, Trommald M, Andersen P. An increase in dendritic spine density on hippocampal CA1 pyramidal cells following spatial learning in adult rats suggests the formation of new synapses. Proceedings of the National Academy of Sciences of the United States of America. 1994; 91:12673–12675. [PubMed: 7809099]

Nakashiba T, Cushman JD, Pelkey KA, Renaudineau S, Buhl DL, McHugh TJ, Rodriguez Barrera V, Chittajallu R, Iwamoto KS, McBain CJ, et al. Young dentate granule cells mediate pattern separation, whereas old granule cells facilitate pattern completion. Cell. 2012; 149:188–201. [PubMed: 22365813]

Okawa H, Hoon M, Yoshimatsu T, Della Santina L, Wong RO. Illuminating the multifaceted roles of neurotransmission in shaping neuronal circuitry. Neuron. 2014; 83:1303–1318. [PubMed: 25233313]

Ostroff LE, Cain CK, Bedont J, Monfils MH, Ledoux JE. Fear and safety learning differentially affect synapse size and dendritic translation in the lateral amygdala. Proceedings of the National Academy of Sciences of the United States of America. 2010; 107:9418–9423. [PubMed: 20439732]

Papes F, Logan DW, Stowers L. The vomeronasal organ mediates interspecies defensive behaviors through detection of protein pheromone homologs. Cell. 2010; 141:692–703. [PubMed: 20478258]

Park H, Popescu A, Poo MM. Essential role of presynaptic NMDA receptors in activity-dependent BDNF secretion and corticostriatal LTP. Neuron. 2014; 84:1009–1022. [PubMed: 25467984]

Pecho-Vrieseling E, Sigrist M, Yoshida Y, Jessell TM, Arber S. Specificity of sensory-motor connections encoded by Sema3e-Plxnd1 recognition. Nature. 2009; 459:842–846. [PubMed: 19421194]

Pieraut S, Gounko N, Sando R 3rd, Dang W, Rebboah E, Panda S, Madisen L, Zeng H, Maximov A. Experience-dependent remodeling of basket cell networks in the dentate gyrus. Neuron. 2014; 84:107–122. [PubMed: 25277456]

Ramiro-Cortes Y, Israely I. Long lasting protein synthesis- and activity-dependent spine shrinkage and elimination after synaptic depression. PloS one. 2013; 8:e71155. [PubMed: 23951097]

Richards DA, Mateos JM, Hugel S, de Paola V, Caroni P, Gahwiler BH, McKinney RA. Glutamate induces the rapid formation of spine head protrusions in hippocampal slice cultures. Proceedings of the National Academy of Sciences of the United States of America. 2005; 102:6166–6171. [PubMed: 15831587]

Schoch S, Deak F, Konigstorfer A, Mozhayeva M, Sara Y, Sudhof TC, Kavalali ET. SNARE function analyzed in synaptobrevin/VAMP knockout mice. Science. 2001; 294:1117–1122. [PubMed: 11691998]

Shatz CJ, Stryker MP. Prenatal tetrodotoxin infusion blocks segregation of retinogeniculate afferents. Science. 1988; 242:87–89. [PubMed: 3175636]

Shen K, Scheiffele P. Genetics and cell biology of building specific synaptic connectivity. Annual review of neuroscience. 2010; 33:473–507.

Shimojo M, Courchet J, Pieraut S, Torabi-Rander N, Sando R 3rd, Polleux F, Maximov A. SNAREs Controlling Vesicular Release of BDNF and Development of Callosal Axons. Cell Rep. 2015; 11:1054–1066. [PubMed: 25959820]

Sretavan DW, Shatz CJ, Stryker MP. Modification of retinal ganglion cell axon morphology by prenatal infusion of tetrodotoxin. Nature. 1988; 336:468–471. [PubMed: 2461517]

Sudhof TC. The presynaptic active zone. Neuron. 2012; 75:11–25. [PubMed: 22794257]

Sudhof TC, Malenka RC. Understanding synapses: past, present, and future. Neuron. 2008; 60:469–476. [PubMed: 18995821]

Tada T, Sheng M. Molecular mechanisms of dendritic spine morphogenesis. Current opinion in neurobiology. 2006; 16:95–101. [PubMed: 16361095]

Takamori S, Holt M, Stenius K, Lemke EA, Gronborg M, Riedel D, Urlaub H, Schenck S, Brugger B, Ringler P, et al. Molecular anatomy of a trafficking organelle. Cell. 2006; 127:831–846. [PubMed: 17110340]

Tom Dieck S, Hanus C, Schuman EM. SnapShot: local protein translation in dendrites. Neuron. 2014; 81:958–958. e951. [PubMed: 24559682]

Tonegawa S, Pignatelli M, Roy DS, Ryan TJ. Memory engram storage and retrieval. Current opinion in neurobiology. 2015; 35:101–109. [PubMed: 26280931]

Trachtenberg JT, Chen BE, Knott GW, Feng G, Sanes JR, Welker E, Svoboda K. Longterm in vivo imaging of experience-dependent synaptic plasticity in adult cortex. Nature. 2002; 420:788–794. [PubMed: 12490942]

Tsai NP, Wilkerson JR, Guo W, Maksimova MA, DeMartino GN, Cowan CW, Huber KM. Multiple autism-linked genes mediate synapse elimination via proteasomal degradation of a synaptic scaffold PSD-95. Cell. 2012; 151:1581–1594. [PubMed: 23260144]

van Versendaal D, Rajendran R, Saiepour MH, Klooster J, Smit-Rigter L, Sommeijer JP, De Zeeuw CI, Hofer SB, Heimel JA, Levelt CN. Elimination of inhibitory synapses is a major component of adult ocular dominance plasticity. Neuron. 2012; 74:374–383. [PubMed: 22542189]

Varoqueaux F, Sigler A, Rhee JS, Brose N, Enk C, Reim K, Rosenmund C. Total arrest of spontaneous and evoked synaptic transmission but normal synaptogenesis in the absence of Munc13- mediated vesicle priming. Proceedings of the National Academy of Sciences of the United States of America. 2002; 99:9037–9042. [PubMed: 12070347]

Verhage M, Maia AS, Plomp JJ, Brussaard AB, Heeroma JH, Vermeer H, Toonen RF, Hammer RE, van den Berg TK, Missler M, et al. Synaptic assembly of the brain in the absence of neurotransmitter secretion. Science. 2000; 287:864–869. [PubMed: 10657302]

Viaene AN, Petrof I, Sherman SM. Synaptic properties of thalamic input to the subgranular layers of primary somatosensory and auditory cortices in the mouse. The Journal of neuroscience : the official journal of the Society for Neuroscience. 2011; 31:12738–12747. [PubMed: 21900553]

Wang CL, Zhang L, Zhou Y, Zhou J, Yang XJ, Duan SM, Xiong ZQ, Ding YQ. Activity-dependent development of callosal projections in the somatosensory cortex. The Journal of neuroscience : the official journal of the Society for Neuroscience. 2007; 27:11334–11342. [PubMed: 17942728]

West AE, Greenberg ME. Neuronal activity-regulated gene transcription in synapse development and cognitive function. Cold Spring Harbor perspectives in biology. 2011:3.

Wiegert JS, Oertner TG. Long-term depression triggers the selective elimination of weakly integrated synapses. Proceedings of the National Academy of Sciences of the United States of America. 2013; 110:E4510–4519. [PubMed: 24191047]

Wiesel TN, Hubel DH. Effects of Visual Deprivation on Morphology and Physiology of Cells in the Cats Lateral Geniculate Body. Journal of neurophysiology. 1963; 26:978–993. [PubMed: 14084170]

Williams ME, Wilke SA, Daggett A, Davis E, Otto S, Ravi D, Ripley B, Bushong EA, Ellisman MH, Klein G, et al. Cadherin-9 regulates synapse-specific differentiation in the developing hippocampus. Neuron. 2011; 71:640–655. [PubMed: 21867881]

Xu T, Yu X, Perlik AJ, Tobin WF, Zweig JA, Tennant K, Jones T, Zuo Y. Rapid formation and selective stabilization of synapses for enduring motor memories. Nature. 2009; 462:915–919. [PubMed: 19946267]

Yu CR, Power J, Barnea G, O'Donnell S, Brown HE, Osborne J, Axel R, Gogos JA. Spontaneous neural activity is required for the establishment and maintenance of the olfactory sensory map. Neuron. 2004; 42:553–566. [PubMed: 15157418]

Zhang Y, Narayan S, Geiman E, Lanuza GM, Velasquez T, Shanks B, Akay T, Dyck J, Pearson K, Gosgnach S, et al. V3 spinal neurons establish a robust and balanced locomotor rhythm during walking. Neuron. 2008; 60:84–96. [PubMed: 18940590]

Zhou Q, Homma KJ, Poo MM. Shrinkage of dendritic spines associated with long-term depression of hippocampal synapses. Neuron. 2004; 44:749–757. [PubMed: 15572107]

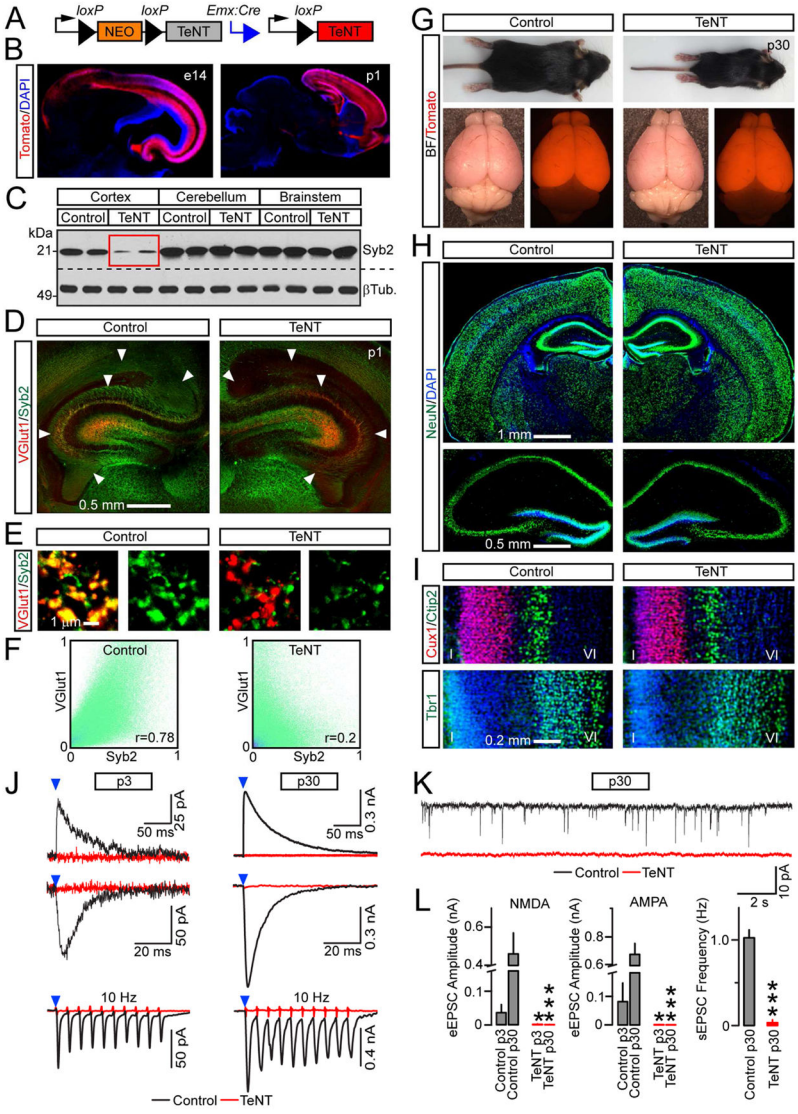


**Figure 1. Characterization of Emx1/TeNT mice**

**(A)** *Emx1*$^{IRES\text{-}Cre}$-inducible expression of TeNT from the *R26*$^{floxstopTeNT}$ allele.

**(B)** Recombinase activity of *Emx1*$^{IRES\text{-}Cre}$ was assessed with *Ai9* tdTomato Cre reporter in brains of e14 embryos and p1 pups. See also Figure S1.

**(C)** Protein extracts from different brain regions of p1 control and Emx1/TeNT mice were tested by immunoblotting for Syb2 and βTubulin.

**(D** to **F)** Brain sections from p1 control and Emx1/TeNT mice were labeled with antibodies against Syb2 and VGlut1.

**(D)** Low-magnification confocal images show a loss of Syb2 in projections of excitatory neurons carrying TeNT (arrows).

**(E)** Individual presynaptic boutons in the CA1.

**(F)** Colocalization of VGlut1 and Syb2 in stratum oriens of the CA1. Pseudo colored pixel intensity graphs and Person's correlation coefficients (r) demonstrate the extent of overlap of two fluorophores in 100$^2$ µm image frames. See also Figure S2.

**(G** to **I)** Control and Emx1/TeNT mice were examined at 4 weeks of age. See also Figure S3.

**(G)** Intact animals and brains. Mice of both genotypes also carried the *Ai9* allele.

**(H** and **I)** Brain sections were imaged after labeling with indicated antibodies.

**(H)** Staining for pan-neuronal marker, NeuN.

**(I)** Distribution of layer-specific excitatory neurons in somatosensory cortex. Top: Cux1 (layers II/III) and Ctip2 (layer V). Bottom: Tbr1 (layer VI).

**(J** to **L)** Glutamatergic neurotransmission in the hippocampus at p3 and p30. EPSCs were monitored from CA1 pyramidal cells in acute slices.

**(J)** Superimposed traces of evoked NMDA (outward) and AMPA (inward) EPSCs that were sampled at +40 and −70 mV, respectively. Schaffer collaterals were stimulated at 0.1 Hz (top) or 10 Hz (bottom, averaged traces from 10 consecutive sweeps are shown). Note the differences in scales.

**(K)** Spontaneous EPSCs at p30.

**(L)** Averaged EPSCs amplitudes and frequencies of spontaneous events. p3: Control, $n = 2$ mice/6 neurons; TeNT, $n = 2/6$. p30: Control, $n = 3/4$; TeNT, $n = 3/5$. $^{*}P < 0.05$; $^{***}P < 0.001$ (Student's *t*-test). See also Table S1.

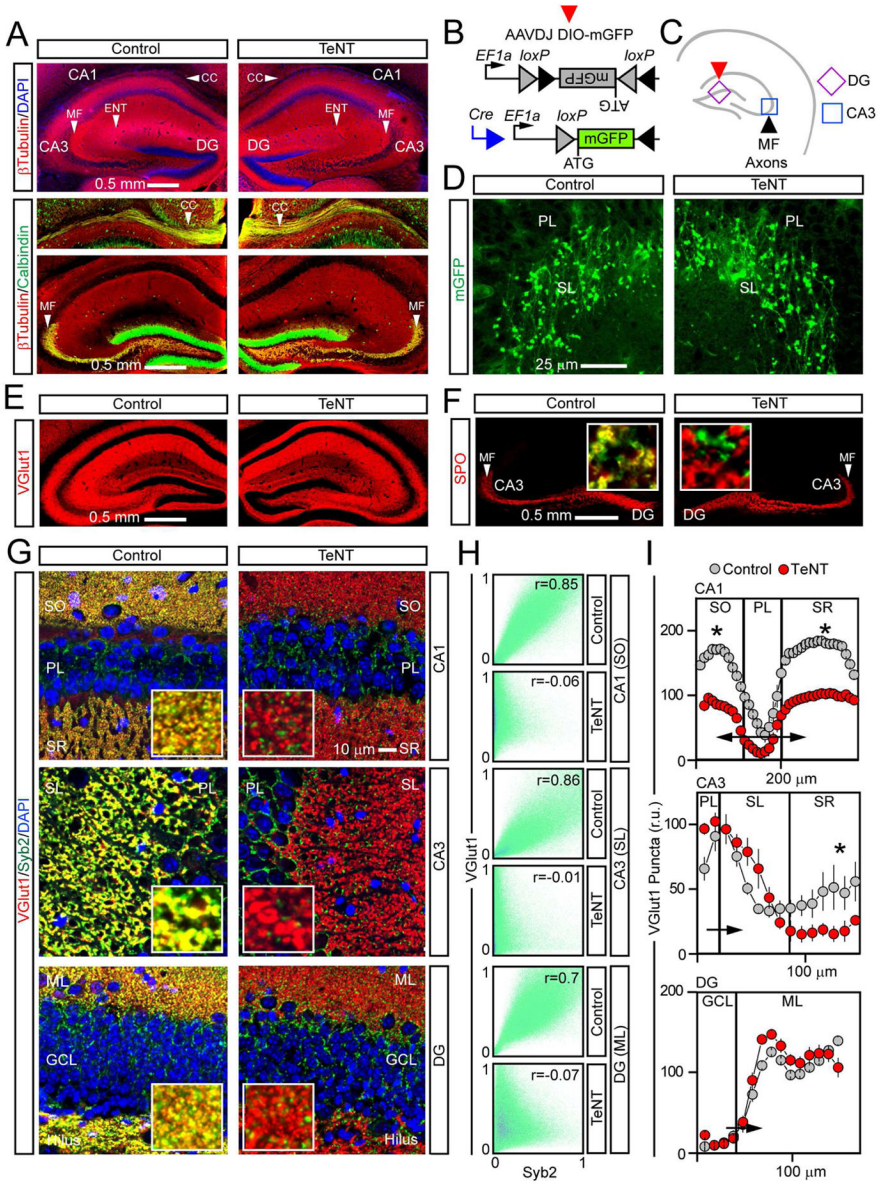


**Figure 2. Presynaptic differentiation of excitatory neurons**

Axons and presynaptic terminals of glutamatergic neurons in hippocampi of 4 weeks old animals.

**(A)** Sections were stained with antibodies against βTubulin and Calbindin. CC = corpus callosum; MF = GC mossy fibers; ENT = axons of layer II entorhinal cortical neurons that terminate in the CA3.

**(B** to **D)** Mossy fibers were tagged *in vivo* with AAVDJ DIO-mGFP.

**(B)** Schematic diagram of reporter induction in excitatory neurons.

**(C)** Sites of mGFP expression and location of inspected axons.

**(D)** GC axons and large mossy fiber terminals (LMTs) in the CA3. SL = stratum lucidum; PL = pyramidal cell layer. See also Figure S5.

**(E** and **F)** Glutamatergic terminals were labeled with antibodies against VGlut1 (E) or a marker of LMTs, SPO (F). Single LMTs in samples co-stained for Syb2 are shown in inserts.

**(G)** Images of the CA1, CA3 and DG in sections that were stained for VGlut1 and Syb2. SO = stratum oriens; SR = stratum radiatum; SL = stratum lucidum; PL = pyramidal cell layer; GCL = granule cell layer; ML = molecular layer.

**(H)** Colocalization of VGlut1 and Syb2 in indicated areas. See also Figure S4.

**(I)** Densities of VGlut1-positive boutons in different sites of the hippocampus. Values from 3 pairs of mice are plotted as mean ± S.E.M. $*P < 0.05$ (Student's *t*-test).

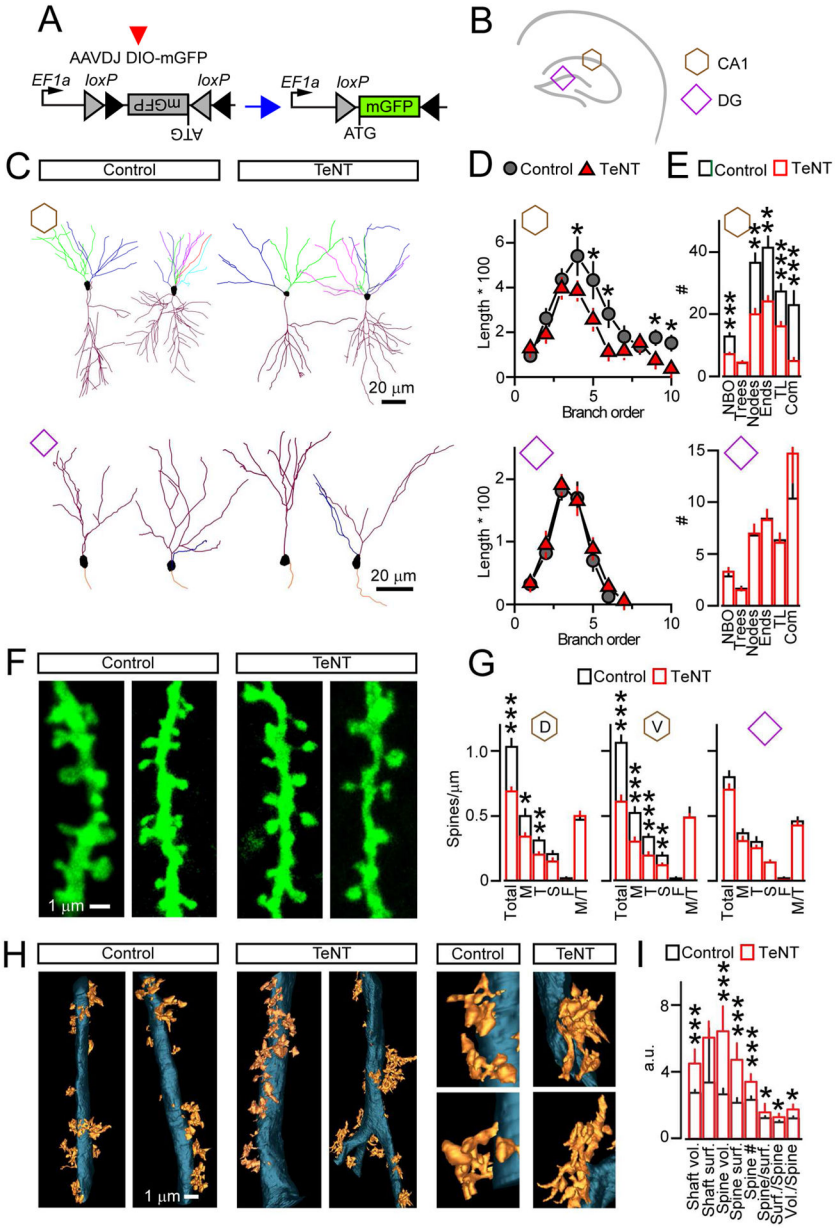


**Figure 3. Dendrites and postsynaptic spines of excitatory neurons**

**(A** to **G)** Pyramidal neurons in the CA1 and dentate GCs were sparsely labeled with AAVDJ DIO-mGFP. Neuronal morphologies were analyzed at p30. Data are annotated as shown in panel B.

**(A** and **B)** Schematics of experimental design with sites of AAV expression.

**(C)** Dendritic trees reconstructed from 3D image stacks. Branches of different order are color-coded.

**(D)** Averaged length of branches of different order (µm * 100).

**(E)** Mean numbers of branch orders (NBO), trees, nodes, ends, tree length (TL, µm * 100), and complexity indexes (Com, a.u. *1000). CA1: Control, $n$ = 3 mice/24 neurons; TeNT, $n$ = 3/20. DG: Control, $n$ = 3/13; TeNT, $n$ = 3/26. See also Figure S5.

**(F)** Images of spines on proximal dendrites of pyramidal cells in the CA1.

**(G)** Linear densities of different spine types on dendrites of CA1 pyramidal and dentate GC neurons. M = mushroom; T = thin; S = stubby; F = filopodia; M/T = ratio of mushroom to total. Dorsal CA1 (D): Control, $n = 3$ mice/15 neurons; TeNT, $n = 3/20$. Ventral CA1 (V): Control, $n = 3/15$; TeNT, $n = 3/15$. DG: Control, $n = 3/21$; NFB, $n = 3/20$.

(**H** and **I**) Spines on proximal dendrites of pyramidal cells in the CA3 were analyzed at p30 by SBEM.

(**H**) Dendritic shafts and spines in stratum lucidum of the CA3.

(**I**) Quantifications of shaft volumes (* $10^{11}$ $nm^3$) and surface areas (* $10^{10}$ $nm^2$), spine volumes (* $10^{10}$ $nm^3$) and surface areas (* $10^8$ $nm^2$), spine numbers, and ratios of spines to dendrite surface, dendrite surface to spine, and dendrite volume to spine (all a.u.). $n = 3$ mice/9–10 reconstructions per genotype.

Graphs are plotted as mean ± S.E.M. *$P < 0.05$; **$P < 0.01$; ***$P < 0.001$ (Student's *t*-test).

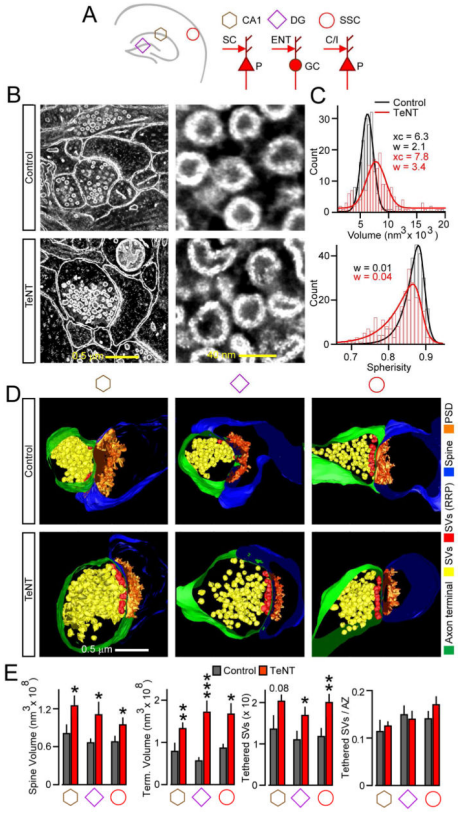


**Figure 4. Architectures of glutamatergic synapses**

Structures of single excitatory synapses in the CA1, DG, and somatosensory cortex of p30 mice were analyzed by SEM.

**(A)** Simplified diagrams of connectivity in examined areas. P = pyramidal neuron; GC = granule cell; C/I = callosal or ascending layer IV afferents; ENT = entorhinal axons; SC = Schaffer collaterals.

**(B)** 2D EM images of synapses (left) and neurotransmitter vesicles (right) in the CA1.

**(C)** Vesicle volumes and spherisity. Histograms were fitted with Gaussian and asymmetric sigmoidal functions, respectively. $n = 270$ vesicles/genotype. xc = center of the distribution; w = width of the distribution. w values are shown for left-skewed slope.

**(D)** 3D views of terminals with opposed spines. Structures are color-coded, as indicated on the right. SV = synaptic vesicle; RRP readily-releasable pool of SVs adjacent to presynaptic active zones (AZ); PSD = postsynaptic density.

**(C)** Quantifications of terminal/spine volumes and tethered pools of SVs, displayed as absolute numbers or normalized to AZ length. Data from 3 mice, 9–12 3D-reconstructions per area/genotype are represented as mean ± S.E.M. $*P < 0.05$; $**P < 0.01$; $***P < 0.001$ (Student's *t*-test). See also Figure S6 and Table S2.